ACS APPLIED MATERIALS & INTERFACES

Research Article

www.acsami.org

Hydrogenated NiO Nanoblock Architecture for High Performance Pseudocapacitor

Ashutosh K. Singh,[†] Debasish Sarkar,*[,†] Gobinda Gopal Khan,[‡] and Kalyan Mandal[†]

[†]Department of Condensed Matter Physics and Material Sciences, S. N. Bose National Centre for Basic Sciences, Block JD, Sector III, Salt Lake City, Kolkata 700 098, India

[‡]Centre for Research in Nanoscience and Nanotechnology, University of Calcutta, Technology Campus, Block JD2, Sector III, Salt Lake City, Kolkata 700 098, India

Supporting Information

ABSTRACT: Supercapacitor electrodes are fabricated with the self-organized 3D architecture of NiO and hydrogenated NiO (H-NiO) nano-blocks (NBs) grown by the facile electrodeposition and high temperature annealing of the Ni foil on Cu substrate. The unique architecture of H-NiO NBs electrode exhibits excellent cycling stability (only 5.3% loss of its initial specific capacitance after 3000 cycles at current density of 1.1 A g^{-1}) along with the high specific and areal capacitance of ~1272 F g^{-1} and 371.8 mF cm^{-2}, respectively at scan rate of 5 mV s^{-1} compared with the pure NiO NBs electrode (~ 865 F g^{-1} and 208.2 mF cm^{-2}, respectively at scan rate of 5 mV s^{-1}). H-NiO NBs electrode also exhibits excellent rate capability; nearly 61% specific capacity retention has been observed when the current density increases from 1.11 to 111.11 A g^{-1}. This electrode offers excellent energy density of 13.51 Wh kg^{-1} and power density of 19.44 kW kg^{-1} even at a high current density of 111.11 A g^{-1}. The superior pseudocapacitive performance of the H-NiO NBs electrode is because of the high electron and ion conductivity of the active material because of the incorporation of hydroxyl groups on the surface of NiO NBs.

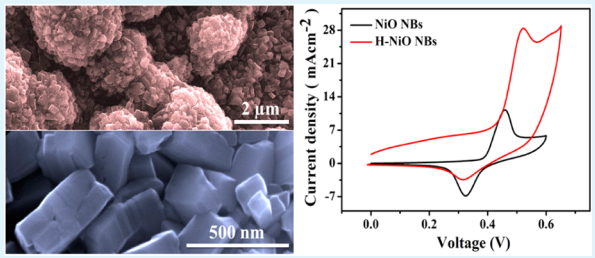

KEYWORDS: *NiO nano-blocks, electrodeposition, hydrogenation, pseudocapacitor, energy storage*

1. INTRODUCTION

Because of growing demand of alternative power sources to reduce environmental pollution caused by fossil fuels, significant research works have been conducted to enhance the efficiency of the alternative energy harvesting materials that transmute energies especially from sun and wind, to a great extent. However, the unavailability of the sunlight at night and unpredictable nature of wind flow have made these alternative energy sources very limited to use. Because of the high demand of portable electronics devices and electric/hybrid vehicles, researchers have worked very hard during the last few decades to find a superior way to store this precious energy so that we can use it in future whenever needed. The invention of electrochemical capacitor, also known as supercapacitor, has become very promising as energy storage device because of their very high energy storage capability as manifested by their high capacitance (almost 20−200 times higher than the conventional capacitors),[1] high power density and long cycle life.[2,3] There are two types of supercapacitors exist based on the energy storage mechanism, known as the electrical double-layer capacitors (EDLCs) and pseudocapacitors. Unlike EDLCs, which store electrical energy by electrostatic accumulation of charges in the electric double-layer near electrode/electrolyte interfaces, the pseudocapacitors, which store electrical energies through surface based faradic reactions, have been found to possess a much higher energy density than that of the EDLCs. However, various transition metal oxides and hydroxides have been investigated as pseudocapacitor, among which $RuO_2 \cdot xH_2O$ have shown the best pseudocapacitive performance,[4,5] though its high cost limits its use for commercial applications. In this context, other transition metal oxide and hydroxides, such as NiO_x,[6−8] $Ni(OH)_2$,[9−11] CoO_x,[12] $Co(OH)_2$,[13,14] MnO_2,[15−17] α-Fe_2O_3,[18,19] V_2O_5,[20,21] Nb_2O_5,[22,23] TiO_2,[24] etc., have been studied extensively in search of the alternative inexpensive electrode material with high capacitive performance.[25] However, nickel oxide has gained extra attention as pseudocapacitor because of its high theoretical specific capacitance (~2573 F g^{-1} within 0.5 V), low cost, environmental friendly nature, and practical availability. There are several reports on the pseudocapcitive performance of different NiO based nanostructures, such as nanoballs,[7] nanowires,[8] thin films,[25,26] nanotubes,[27] nano columns[28] etc. having a specific capacitance within ~250 to 950 F g^{-1}, though much less than the theoretical value and also less than that obtained for RuO_2 or MnO_2 based pseudocapacitors. Therefore, the improvement of the capacitive performance of NiO based pseudocapacitors as electrode materials has become a focus of intense research interest. Recent development of the nanostructured materials

Received: November 7, 2013
Accepted: March 6, 2014
Published: March 6, 2014

and detail investigation of the charge storage mechanism within these nanostructured pseudocapacitive materials give us a clue in this respect. In case of pseudocapacitors, it has been found that, during charge storage via faradic reactions the electron and ion transfer from the electrolyte to the electrode materials and vice versa significantly depends on several properties of the electrode material, such as surface area, electronic conductivity, redox activity of the electrode materials, etc. Therefore, we can expect that designing of a nanostructured electrode having extremely high specific surface area (such as nanowires, nanotubes, nanoblocks, mesoporous nanostructures, etc.) of a highly redox active material will result high specific capacitance with high energy and power densities by allowing fast ion and electron transport on the surface and also into the electrode materials from electrolyte. Furthermore, higher electronic conductivity of the electrode materials will ease faster transport of electrons through it to the current collectors, which would enhance their capacitive performance significantly. In addition to this, the introduction of some highly active oxygen containing functional groups like hydroxyl (−OH) and carboxyl (−COOH) groups on the nanostructured electrode surface has been found to be more effective for enhancing capacitance by producing steric hindrance or charge bias effects.[29]

In this background, we have fabricated hydrogenated 3D NiO nanoblocks (NBs) on Cu substrate by combining electrodeposition and annealing methods. This type of architecture of electrode materials is more preferable because here, it is not required to mix the active materials with some highly conductive materials like carbon to prepare the electrode. This special electrode designed based on nanostructures also has the following advantages: (i) the as grown NiO NBs have large surface area that would facilitate faster ion intercalation/de-intercalation into the electrodes leading to higher capacitance, (ii) NiO is highly redox active with the high value of theoretical specific capacitance and the presence of conductive Ni,[30] at the bottom would serve as the fast path for electron migration to the current collector (here Cu substrate), and (iii) hydrogenation of the nanoblocks will introduce hydroxyl groups of the surface and subsurface regions of NiO nanoblocks, which can enhance its capacitive performance significantly by changing the conductivity of the active materials. As expected, the specific capacitance of the pseudocapacitor electrodes made of as grown NiO NBs is found to be ∼895 F g^{-1} at a current density of 1.11 A g^{-1}, which becomes ∼1336 F g^{-1} after hydrogenation. Moreover, both of the materials show relatively good rate capability, high energy and power performance and even long cycle stability (∼94% retention after 3000 cycles) which make them auspicious candidates for fabricating high performance pseudocapacitor electrodes.

2. EXPERIMENTAL SECTION

2.1. Reagents. Copper foil (99.98 % pure, 0.1 mm thick), nickel sulphate hexahydrate ($NiSO_4·6H_2O$, 99.99 % pure), boric acid (H_3BO_3, 99.9 % pure), potassium hydroxide (KOH, 99.9 % pure), and sodium hydroxide (NaOH, 99.9 % pure) were purchased from Sigma-Aldrich. All chemicals were of analytical grade and were used without further purification.

2.2. Synthesis of NiO NBs and Hydrogenated NiO (H-NiO) NBs. The high-density 3D architecture of NiO NBs were synthesized by the high-temperature oxidation of the highly rough metallic Ni thin film prepared by the metal substrate assisted electrochemical deposition technique. Software controlled three-electrode electrochemical cell and a power supply (potentiostat AutoLab-30) was used for the electrochemical deposition of Ni thin film. A high-purity platinum wire and an Ag/AgCl electrode were used as the counter and reference electrodes, respectively. Ni thin film with rough surface was grown on the pure Cu substrate using the aqueous solution of 0.57 M $NiSO_4·6H_2O$, 0.32 M H_3BO_3, and 0.15 M NH_4OH as electrolyte at room temperature. Here, boric acid and ammonium hydroxide were used as a buffer to maintain the pH of the electrolyte around 3.5 and also to control the electrodeposition process. The deposition of the Ni thin film was conducted for 30 minutes by using a DC voltage of −0.95 V, following linear sweep voltammetry (LSV) results. The Ni thin film grown on the Cu substrate was finally oxidized to form NiO NBs by heating them at 450°C for 30 minutes in oxygen atmosphere. The H-NiO NBs were obtained by annealing the NiO NBs in hydrogen atmosphere at temperature of 400°C for 20 minutes. During this process, the exposed side of Cu substrate (on which Ni was not deposited) was also oxidized to some extent to form a thin layer (∼12 μm) of CuO (Supporting information, Figure S1). However, for making the electrical contact, the oxidized portion of Cu substrate was removed carefully by keeping the other side of the Cu substrate (the side containing NiO NBs) untouched. The NiO or H-NiO film thickness was found to be ∼3 μm. The mass of the active electrode material was measured by using a microbalance having an accuracy of 0.1 μg. The loading density of the NiO and H-NiO NBs electrodes were 0.327 and 0.314 mg/cm^2, respectively.

2.3. Materials Characterization. The crystal structure of the as prepared NiO and H-NiO NBs were analysed by X-ray diffraction (XRD, Panalytical X'Pert Pro diffractometer). The chemical and elemental composition of the NBs was investigated by energy dispersive X-ray (EDAX) and X-ray photoelectron spectroscopy (XPS). The morphology and the structure of the 3D arrays of NiO and H-NiO NBs were studied by field emission scanning electron microscope (FESEM, FEI Quanta-200 Mark-2).

2.4. Electrochemical Measurements. A software controlled three electrode cell (potentiostat AutoLab-30) was used for all electrochemical measurements of the as prepared supercapacitor electrodes. The cell consists of the as-prepared samples as the working electrode, Ag/AgCl electrode as the reference electrode, Pt wire as the counter electrode and 1 M KOH solution as electrolyte, at room temperature. Cyclic voltammetry (CV) studies were performed at different scan rates varied from 5 to 100 mV s^{-1}. Galvanostatic (GV) charge/discharge measurements were conducted at various current densities varied from 1.11 to 111.11 A g^{-1} to evaluate the specific capacitance, power density and energy density. A potential window in the range from 0 to 0.6 V was used in all these CV and GV measurements. Electrochemical impedance spectroscopy (EIS) was carried out to prove the capacitive performance at open circuit potential in 1 M KOH within a frequency range of 0.1−10^5 Hz. The constant current charge/discharge method was also employed to test the long-rate capability of the electrode materials. The long-cycle stability of the electrodes was tested by galvanostatic charge/discharge method during 3000 cycles at a current density of 1.11 A g^{-1}.

3. RESULTS AND DISCUSSION

3.1. Morphology, Crystallography, and Chemical Composition. The scheme of the preparation of the arrays of H-NiO NBs is shown in Figure 1. Details of the synthesis and fabrication of H-NiO NBs are already given in the Experimental Section.

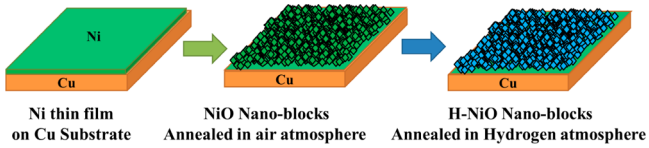

Figure 1. Schematic of the preparation of NiO and H-NiO NBs electrodes on Cu substrates.

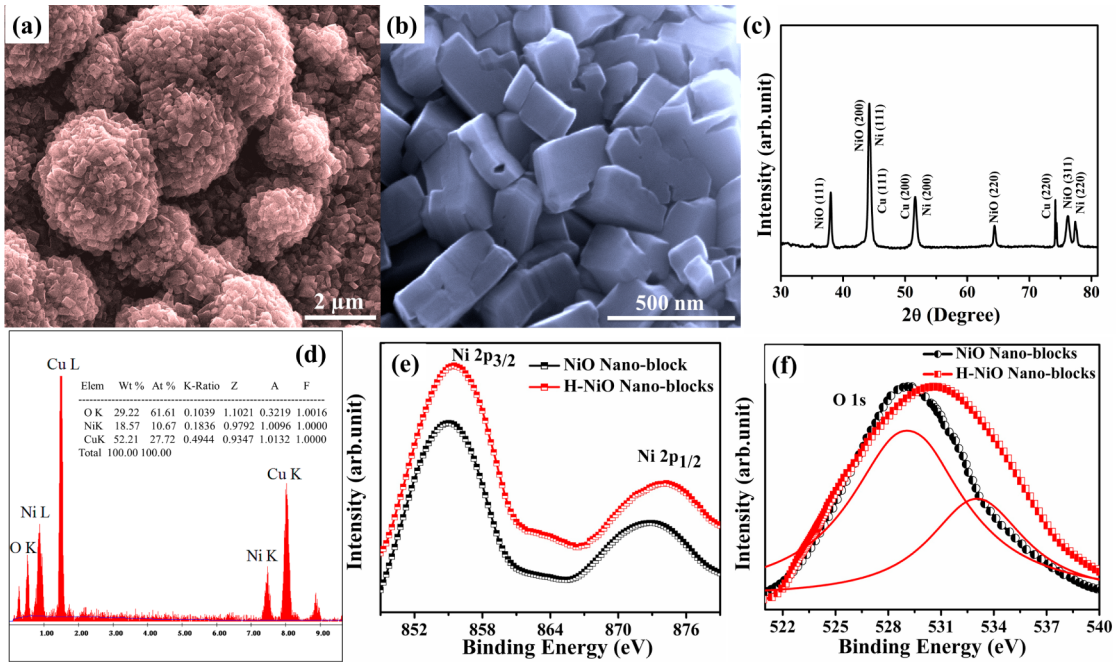

Figure 2. (a, b) FESEM micrographs of the as prepared H-NiO NBs. (c) XRD pattern of the as-prepared H-NiO NBs. (d) EDAX spectrum of the as-prepared H-NiO NBs. The XPS spectra for the (e) Ni 2p and (f) normalized O 1s core level of the as-prepared NiO and H-NiO NBs.

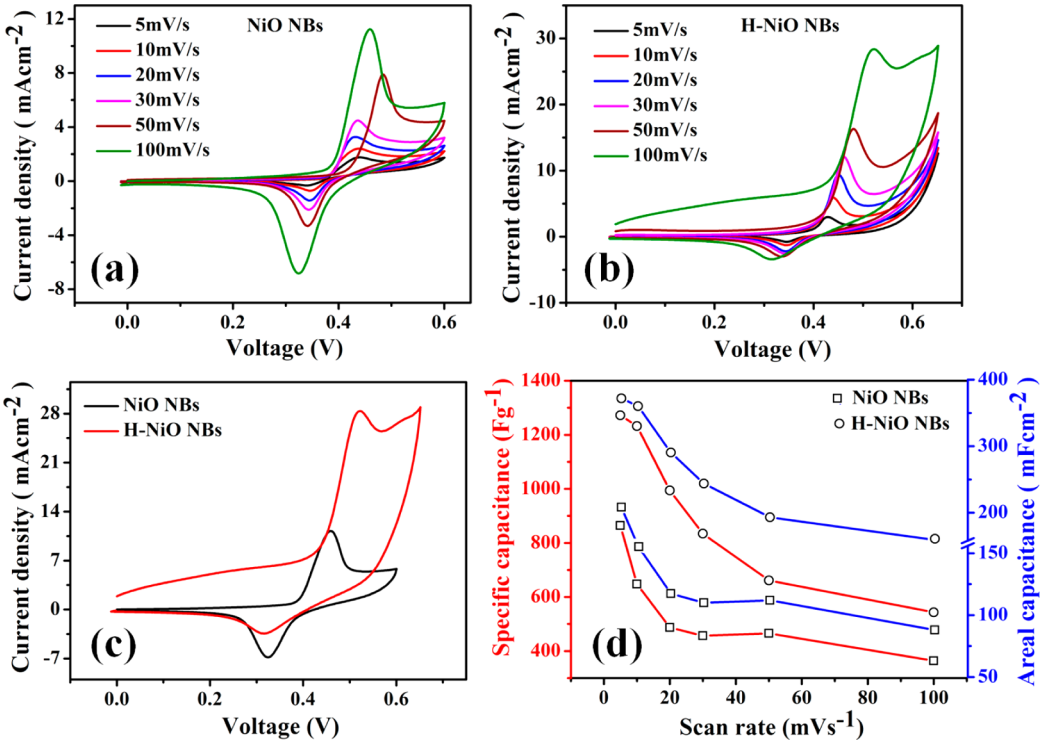

Figure 3. Cyclic voltammetry curves of the as-prepared (a) pure NiO and (b) H-NiO NBs electrode at different scan rates in a 1 M KOH solution at room temperature. (c) Comparison between the CV curves of pure NiO and H-NiO NBs at scan rate of 100 mV s^{-1}. (d) Variation of specific and areal capacitance as a function of scan rate of pure NiO and H-NiO NBs electrodes.

Figure 2a shows the FESEM micrograph of the as-prepared 3D arrays of H-NiO NBs grown on Cu substrate. It is evident from this image that the surface of the as prepared nanostructure is very rough, which can also be seen from the magnified FESEM image (Figure 2b). It is found that the morphology of the as grown NiO NBs remains unchanged after hydrogenation. The 3D structure of the NiO NBs arises during the conversion of the as grown rough Ni thin film (Supporting information, Figure S2) into NiO via high temperature oxidation. The comparison between Figure 2a and Supporting Information Figure S2 clearly demonstrates that the surface area of the as grown 3D NiO NBs is significantly higher than that of the as grown Ni thin film. Though the shape and size of the grown NiO nanoblocks are irregular in nature, however, the

dx.doi.org/10.1021/am404995h | ACS Appl. Mater. Interfaces 2014, 6, 4684−4692

average dimension of the single NiO nanoblock is found to be around 250 × 200 × 125 nm.

The XRD pattern of the as-prepared H-NiO NBs, shown in Figure 2c, indicates the polycrystalline nature of the as-grown NBs. The diffraction pattern consists of peaks that correspond to the pure fcc Ni, cubic NiO, and also the metallic Cu substrate underneath. The characteristic peaks at 2θ = 37.5, 43.3, and 63.9 degrees in the XRD pattern represent the (111), (200), and (220) crystalline faces of NiO with cubic texture, respectively.[27,31] The presence of Ni (200) peak in the XRD pattern is due to the presence of some unoxidized Ni at the deepest portion of the Ni thin film. Figure 2d depicts the EDAX spectrum of the H-NiO NBs, which clearly shows the presence of Ni and O in the NiO, whereas the peak for Cu appears from the substrate. In Figure 2e, the XPS core level peaks of H-NiO NBs shows the Ni $2p_{3/2}$ and Ni $2p_{1/2}$ located at 855 and 873.9 eV, respectively, with an energy separation of 18.9 eV, are in good agreement with reported data of Ni $2p_{3/2}$ and Ni $2p_{1/2}$ in NiO, which also confirms that Ni is in +2 oxidation state.[31,32] Figure 2f shows the O 1s core level spectra of NiO and H− NiO NBs. The O 1s band for H-NiO NBs becomes broader compared with that of the pure NiO NBs. The O 1s band in the H-NiO NBs could be deconvoluted into two peaks located at 529.1 and 533.1 eV (see Figure 2f), whereas the pure NiO NBs exhibits a single peak located at 530.7 eV. The low energy peak (at 530.7 eV) can be ascribed to the formation of O−Ni bond in NiO,[31,33] whereas the peak at higher binding energy (at 533.1 eV) is attributed to the Ni−OH bond.[10,33] Thus, XPS studies confirm the incorporation of hydroxyl groups on the surface and the subsurface region of the NiO NBs through hydrogenation.

3.2. Electrochemical Analysis. Figure 3a and b shows the CV measurement curves of the two electrodes at different scan rates ranging between 5 to 100 mV s^{-1} within the voltage window of 0 to 0.6 V, at room temperature. The shape of the CV curves of both the electrodes clearly reveals the pseudocapacitive behaviour of the electrodes which is totally different from that of the double layer capacitors. CV curves show one strong redox peak (one oxidation and one reduction peaks) at every scan rates, which are corresponding to the surface oxidation/reduction reactions as shown in the eq 1.[34] The oxidation peak is due to the conversion of NiO/$Ni(OH)_2$ to NiOOH and the reduction peak is simply because of the reverse reaction. The redox peaks show the Faradaic pseudocapacitive property based on the surface redox mechanism between Ni^{2+} and Ni^{3+}.

$$NiO + OH^- \leftrightarrow NiOOH + e^-$$

and

$$Ni(OH)_2 + OH^- \leftrightarrow NiOOH + H_2O + e^- \quad (1)$$

In addition, because of the very high surface area and the fast ionic/electronic diffusion rate during the Faradic redox reactions at the surface, both the NiO and H-NiO NBs electrodes show very prominent electrochemical properties as supercapacitor.[35,36] With the increase of scan rate, the potential and the current at the oxidation/reduction peaks shifted more towards the positive and negative axes, respectively, which is because of an increase of the internal diffusion resistance within the pseudocapacitive material with an increase in scan rate.[37,38]

Furthermore, the oxidation and reduction peaks of the NiO NBs electrode are nearly symmetrical throughout the scan range 5−100 mV s^{-1}, indicating good reversibility of redox reaction at the electrode surface.[39] But the redox peaks of H-NiO NBs electrode are asymmetric in nature; though it exhibits higher capacitive behaviour as evident from the higher area (Figure 3c) under their corresponding CV curves as compare to the CV curves of NiO NBs electrodes.

The current response is found to increase almost proportionally with increasing scan rates, which suggests that the rates of electronic and ionic transport are not limited at higher scan rates.[40] The linear relation observed between the peak current (I) of CV loops at different scan rates with the square root of scan rate voltage ($f^{1/2}$) confirms a fast electron transfer rate during the redox reactions, and thus it is evident that these redox reactions are diffusion-controlled process rather than a kinetic one (Supporting information, Figure S3).[41,42] Figure 3c shows a nearly 2.5 times enhancement in the current density in the CV curve of the H-NiO NBs electrode in comparison with the pure NiO NBs electrode at the scan rate of 100 mV s^{-1}.

The calculated areal (C_a, mF cm^{-2}) and specific (C_{sp}, F g^{-1}) capacitance of both the electrodes as a function of scan rate are shown in Figure 3d. The C_a and C_{sp} of the NiO NBs based electrodes are calculated using the equations[19,43,44]

$$C_a = \frac{I}{fA} \quad (2)$$

and

$$C_{sp} = \frac{I}{fm} \quad (3)$$

where I (A) is the average cathodic current of the CV loop, f (V s^{-1}) is the scan rate, A (cm^2) is the area of the working electrode, and m (g) is the mass of the redox active material. The values of the C_a and C_{sp} for NiO NBs electrode are found to be 208.2 mF cm^{-2} and 864.65 F g^{-1}, respectively, at a scan rate of 5 mV s^{-1}. Whereas the C_a and C_{sp} of H-NiO NBs electrode have been found to increase significantly to the values 371.8 mF cm^{-2} and 1271.93 F g^{-1}, respectively, at the scan rate of 5 mV s^{-1}, after the hydrogenation treatment. Figure S4 in Supporting Information shows the variation of specific and areal capacitance as a function of scan rate for pure NiO and H-NiO NBs electrodes with the measurement error bars, while the measurements are conducted for three replicated electrodes for each sample. The noteworthy enhancement of the capacitive property of the H-NiO NBs electrode is due to the absorption of hydroxyl group on the surface of the NiO NBs having large surface area with high stability. Here, the value of specific capacitance for H-NiO NBs is found to be remarkably higher than that of the other reported NiO based supercapacitors like, NiO thin films (~309 F g^{-1}),[45] NiO nanotubes (~266 F g^{-1}),[46] NiO_x nanoball (~951 F g^{-1}),[10] NiO nanocolumns (~309 F g^{-1}),[28] mesoporous NiO nanotubes (~409 Fg^{-1}),[27] hierarchical spherical porous NiO (~710 F g^{-1}),[47] Ni−NiO core−shell (~128 and 149 F g^{-1}),[39,48] NiO/Co_2O_3 core/shell NWs (~835 F g^{-1}),[49] and monolithic NiO/Ni nanocomposites (~905 F g^{-1}).[50] As shown in Figure 3d, the values of C_a and C_{sp} decrease for both the electrodes with the increase of scan rate, which is because of the limitation of reaction kinetics at the electrodes at higher scan rates.[51] The value of C_{sp} of the H-NiO and NiO NBs drops from 1271.93 to 543.63 F g^{-1} and 864.65 to 363.83 F g^{-1}, respectively, with the increase of the scan rate. In addition, the value of C_a also drops from 371.8 to 159 mF cm^{-2} and 208.2 to 88 mF cm^{-2} for H-NiO and NiO NBs, respectively, when the scan rate increases from 5 to 100 mV s^{-1}.

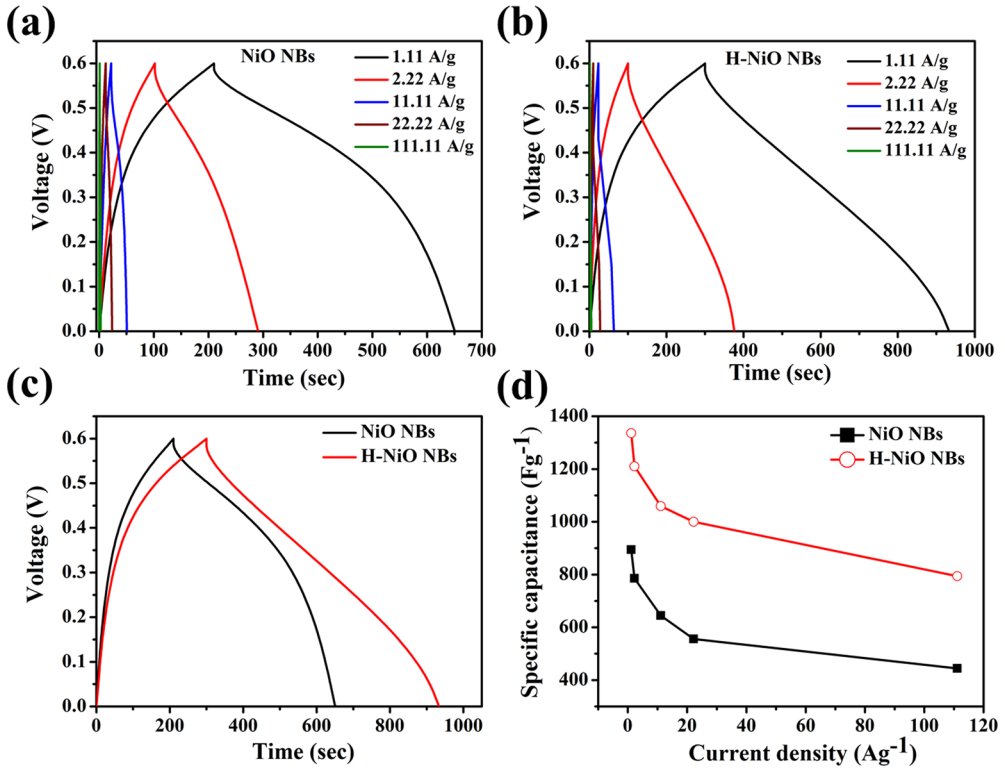

Figure 4. Constant current charge/discharge curves of the as-prepared (a) pure NiO and (b) H-NiO NBs electrodes at different current density. (c) Comparison between the charge/discharge curves of the pure NiO and H-NiO NBs electrodes at a current density of 1.11 A g^{-1}. (d) Variation of the specific capacitance of the electrodes as a function of current density.

The GV charge/discharge tests of both the electrodes performed within a stable potential window of 0−0.6 V under different charge/discharge current densities ranging between 1.11 to 111.11 A g^{-1} are shown in Figure 4a and b, to demonstrate the improved capacitive performance of the electrodes. The potential-time plots exhibiting asymmetric charge/discharge profiles for both NiO and H-NiO NBs electrodes, characterized by slow discharging process as compare to the charging, even at the high current density of 111.11 A g^{-1}. This slow rate of discharging exhibits higher coulombic efficiency (>100 %) for both type of electrodes, which can be explained by eq 1. In discharging process only a part of NiOOH gains electron and get reduced into NiO, while in charging process NiO loses electron and completely oxidized into NiOOH. Since, NiOOH is partially converted into NiO during reduction, the unconverted NiOOH holds the electrons during discharging and thus the discharging takes longer time.[52] Figure 4c showing the enhancement in the discharging time of H-NiO NBs electrode over NiO NBs electrode at the current density of 1.11 A g^{-1}, indicates the enhanced pseudocapacitive behaviour of NiO NBs electrode after hydrogenation. The variation of C_{sp} of both the electrodes is shown in Figure 4d as a function of current density.

The values of C_{sp} are calculated from the charging/discharging curves using the equation[53]

$$C_{sp} = \frac{I\Delta t}{m\Delta V} \tag{4}$$

;where I (A) is the discharge current, Δt (s) is the discharge time consumed in the potential range of ΔV (V), m (g) is the mass of the active material (or mass of the electrode materials), ΔV is the potential window, and I/m is the discharge current density. The maximum values of C_{sp} are found to be 1336.18 and 895.05 F g^{-1} for H-NiO and NiO NBs electrodes, respectively, at the low current density of 1.11 A g^{-1}. Decrement in the specific capacitance has been observed with the increase of current density, although this decrement gets saturated at higher current densities. However, nearly 61% and 49% specific capacitance retention has been observed in H-NiO and NiO NBs electrode, respectively, at a higher current density of 111.11 A g^{-1}. Figure S5 in Supporting Information shows the variation of specific capacitance as a function of current density for pure NiO and H-NiO NBs electrodes calculated from GV curves with the measurement error bars, while the measurements are performed for three replicated electrodes for each pasudocapacitive material.

At lower current densities, ions can penetrate into the inner-structure of electrode materials, having access to almost all available pores of the electrode, but at higher current densities, an effective utilization of the material is limited only to the outer surface of the electrodes. This results in the reduction of the values of specific capacitance at higher current densities. At current densities above 2.22 A g^{-1}, specific capacitance tends to stabilize. This higher value of retention in the specific capacitance of the electrodes indicates relatively good high-rate capability of these electrodes. Impressively, in case of charging/discharging process the capacitance retention of the electrodes is found much higher than that observed from the CV analysis. This is because of the fact that the ion and electron have more time to diffuse through the rough surface of the electrode during the redox reaction.[54,55]

The energy (E) and the specific power (P) densities of both the electrodes are calculated by using the equations[56]

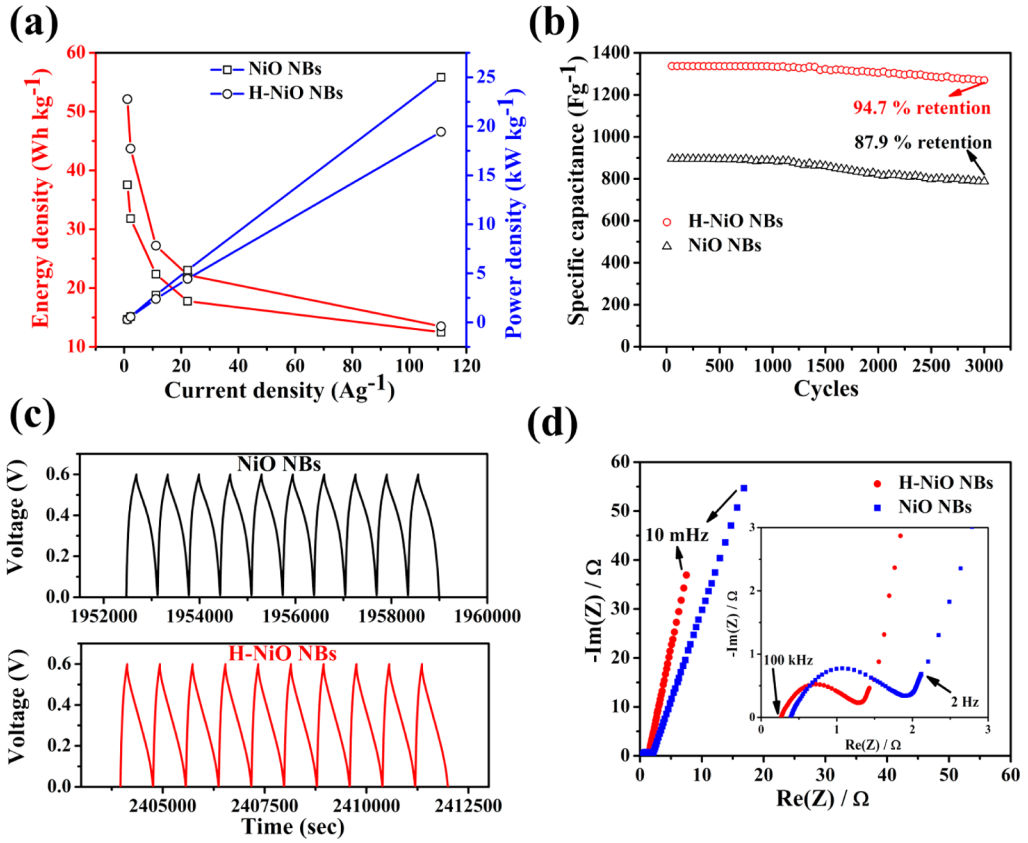

Figure 5. (a) Variation of energy and power densities with charge/discharge current densities for NiO and H-NiO NBs electrodes. (b) The cycling performance of both NiO and H-NiO NBs electrodes showing the capacitance retention after 3000 cycles using a charge/discharge current density of 1.11 A g^{-1}. (c) The last 10 cycles of the galvanostatic charge/discharge curves of NiO and H-NiO NBs electrodes. (d) Electrochemical impedance spectroscopy (Nyquist) plots for the supercapacitors based on NiO and H-NiO NBs electrodes. The inset of panel c shows the Nyquist plot of both the electrodes at high frequency range.

$$E = \frac{1}{2} C_{sp} (\Delta V)^2 \tag{5}$$

and

$$P = \frac{E}{\Delta t} \tag{6}$$

where E (Wh kg^{-1}), C_{sp} (F g^{-1}), ΔV (V), Δt (s), and P (kW kg^{-1}) are the energy density, specific capacitance, the potential window of discharge, time of discharge, and power density, respectively.

Figure 5a shows that the energy density of H-NiO and NiO NBs electrode decreases from 52.13 to 13.51 and 37.56 to 12.49 Wh kg^{-1}, respectively, whereas the power density for the same increases from 0.28 to 19.44 and 0.31 to 24.4 kW kg^{-1}, respectively, as the discharge current density increased from 1.11 to 111.11 A g^{-1}. This indicates the potential of the electrodes for application in electrochemical supercapacitors. The above mentioned values of energy and power density of both the electrodes are better than many other NiO based electrodes reported previously.[10,27,28,45−48]

The cyclic performance of both the NBs electrodes, which includes cycling life and specific capacitance retention of the supercapacitors are shown in Figure 5b, tested over 3000 cycles carried out at a current density of 1.11 A g^{-1}. The capacitance losses of H-NiO and NiO NBs electrodes after 3000 cycles are about 5.3% and 12.1%, respectively, which are found to be better than that of the previously reported NiO based supercapacitors. Both the electrodes exhibit good long term electrochemical stability and high specific capacitance retention after a long cycle test in KOH solution, which are very important requirements for supercapacitors. Figure 5c shows the charge/discharge profiles of the last 10 cycles obtained from the long cycling tests for both the electrodes that remain almost unchanged during the cycles.

The electrical conductivity and ion transfer of the supercapacitor electrodes has been investigated further by electrochemical impedance spectroscopy (EIS). Figure 5d shows the Nyquist impedance plots for the H-NiO and NiO NBs pseudocapacitors. EIS has been carried out in 1 M KOH solution within a frequency range of 0.1−10^5 Hz at amplitude of 10 mV versus the open circuit potential. The EIS spectra are divided into three distinct regions based on the order of decreasing frequencies. The slope of the EIS curve in the low frequency range reflects the Warburg resistance, which describes the diffusion rate of redox material in the electrolyte. The higher value of slope in case of H-NiO NBs electrode over NiO NBs electrode indicates higher electrolytic ion diffusion within the H-NiO NBs structure.[57] The phase angle of the impedance plot of the H-NiO and NiO NBs electrodes found to be higher than 45° in the low frequency range suggesting that the electrochemical capacitive behaviour of both the electrodes is controlled by diffusion process. The shorter line at lower frequency correlates to the shorter variations in ion diffusion path and easier movement of the ions within the pores. The diameter of semicircle in the high frequency range

dx.doi.org/10.1021/am404995h | ACS Appl. Mater. Interfaces 2014, 6, 4684−4692

represents the charge transfer resistance (R_{ct}) of the electrode material resulting from the diffusion of electrons. Here, the value of R_{ct} for H-NiO electrode (1.02 Ω) is smaller than that of the NiO electrode (1.51 Ω), which indicates that H-NiO NBs are ideal for fast ion and electron transport, because the larger diameter semicircle reflects higher charge-transfer resistance value. The intercept on the real axis in the high frequency range provides the equivalent series resistance (ESR), which comprises of the bulk resistance of the electrolyte, the inherent resistances of the electro active material and the contact resistance at the interface between electrolyte and electrode.[58] The value of ESR calculated for H-NiO and NiO NBs electrodes are 0.263 and 0.389 Ω, respectively, which again suggests higher electrical conductivity of H-NiO over NiO NBs electrode. These studies indicate that the H-NiO NBs electrode has low ion diffusion resistance, which can be attributed to the incorporation of hydroxyl groups on the surface of NiO NBs after hydroganetion.

4. CONCLUSION

In summary, large surface area electrodes made of 3D architecture of NiO and H-NiO nano-blocks have been successfully fabricated by the controlled electrodeposition followed by high temperature thermal treatment of the Ni thin film grown on the Cu substrate. Both the electrodes have been demonstrated based on their electrochemical performance as supercapacitor, where the H-NiO NBs exhibit remarkably superior pseudocapacitive performance. It has been found that the incorporation of hydroxyl groups on the surface/subsurface of NiO NBs through hydrogenation improving the electrochemical activity of the H-NiO NBs electrode as pseudocapacitor. In addition, H-NiO NBs serve as the ideal pathway for fast ion/electron diffusion, whereas the conductive Ni and Cu layer at the underneath work as the efficient current collector. The H-NiO NBs electrode exhibits high specific capacitance (1272 F g^{-1}), energy density (52.13 Wh kg^{-1}), power density (19.44 kW kg^{-1}) and excellent cycling stability (only 5.3% loss of its initial specific capacitance after 3000 cycles at current density of 1.11 A g^{-1}). H-NiO NBs electrode also exhibits excellent rate capability, where nearly 61% specific capacity retention has been found when the current density increases from 1.11 to 111.11 A g^{-1}. Here, an easy and low cost fabrication technique of the surface modified unique nano-architecture of NiO has been demonstrated, which could remarkably improve the electrochemical performance of this type of transition metal oxide based electrodes for a new class of high-performance materials for pseudocapacitors.

■ ASSOCIATED CONTENT

Supporting Information

FESEM micrographs of the as prepared Ni thin film on Cu substrate, peak current (I) vs square root of scan rate (f) plot for both types of capacitors, and the error bars in measuring specific and areal capacitance. This material is available free of charge via the Internet at http://pubs.acs.org.

■ AUTHOR INFORMATION

Corresponding Author

*E-mail: deb.sarkar1985@gmail.com or debasish1985@bose.res.in.

Author Contributions

A.K.S., D.S., and G.G.K. contributed equally to this work.

Notes

The authors declare no competing financial interest.

■ ACKNOWLEDGMENTS

The above work was supported by the Board of Research in Nuclear Sciences (BRNS), Government of India funded project 2009/37/16/BRNS. The authors, Ashutosh K. Singh and Debasish Sarkar thank S. N. Bose National Centre for Basic Sciences, India, for providing financial support through research fellowship. Author Gobinda Gopal Khan is thankful to Department of Science and Technology (DST), Government of India, for providing research support through "INSPIRE Faculty Award" (IFA12-ENG-09).

■ REFERENCES

(1) Lang, J. W.; Kong, L. B.; Wu, W. J.; Luo, Y. C.; Kang, L. Facile approach to prepare loose-packed NiO nano-flakes materials for supercapacitors. *Chem. Commun.* **2008**, *35*, 4213−4215.

(2) Miller, J. R.; Simon, P. Electrochemical capacitors for energy management. *Science* **2008**, *321*, 651−652.

(3) Simon, P.; Gogotsi, Y. Materials for electrochemical capacitors. *Nat. Mater.* **2008**, *7*, 845−854.

(4) Hu, C. C.; Chang, K. H.; Lin, M. C.; Wu, Y. T. Design and tailoring of the nanotubular arrayed architecture of hydrous RuO_2 for next generation supercapacitors. *Nano Lett.* **2006**, *6*, 2690−2695.

(5) Chen, P. C.; Chen, H. T.; Qiu, J.; Zhou, C. W. Inkjet printing of single-walled carbon nanotube/RuO_2 nanowire supercapacitors on cloth fabrics and flexible substrates. *Nano Res.* **2010**, *3*, 594−603.

(6) Wang, B.; Chen, J. S.; Wang, Z.; Madhavi, S.; Lou, X. W. Green synthesis of NiO nanobelts with exceptional pseudo-capacitive properties. *Adv. Energy Mater.* **2012**, *2*, 1188−1192.

(7) Lee, J. W.; Ahn, T.; Kim, J. H.; Ko, J. M.; Kim, J. D. Nanosheets based mesoporous NiO microspherical structures via facile and template-free method for high performance supercapacitors. *Electrochim. Acta* **2011**, *56*, 4849−4857.

(8) Singh, A. K.; Sarkar, D.; Khan, G. G.; Mandal, K. Unique hydrogenated Ni/NiO core/shell 1D nano-heterostructures with superior electrochemical performance as supercapacitors. *J. Mater. Chem. A* **2013**, *1*, 12759−12767.

(9) Wang, H. L.; Casalongue, H. S.; Liang, Y. Y.; Dai, H. J. $Ni(OH)_2$ nanoplates grown on graphene as advanced electrochemical pseudocapacitor materials. *J. Am. Chem. Soc.* **2010**, *132*, 7472−7477.

(10) Tian, X.; Cheng, C.; Qian, L.; Zheng, B.; Yuan, H.; Xie, S.; Xiao, D.; Choi, M. M. F. Microwave-assisted non-aqueous homogenous precipitation of nanoball-like mesoporous α-$Ni(OH)_2$ as a precursor for NiO_x and its application as a pseudocapacitor. *J. Mater. Chem.* **2012**, *22*, 8029−8035.

(11) Chen, H.; Hu, L.; Yan, Y.; Che, R.; Chen, M.; Wu, L. One-step fabrication of ultrathin porous nickel hydroxide-manganese dioxide hybrid nanosheets for supercapacitor electrodes with excellent capacitive performance. *Adv. Energy Mater.* **2013**, *3*, 1636−1646.

(12) Deng, M. J.; Huang, F. L.; Sun, I. W.; Tsai, W. T.; Chang, J. K. An entirely electrochemical preparation of a nano-structured cobalt oxide electrode with superior redox activity. *Nanotechnology* **2009**, *20*, 175602−175606.

(13) Wu, C. M.; Fan, C. Y.; Sun, I. W.; Tsaic, W. T.; Chang, J. K. Improved pseudocapacitive performance and cycle life of cobalt hydroxide on an electrochemically derived nano-porous Ni framework. *J. Power Sources* **2011**, *196*, 7828−7834.

(14) Jiang, J.; Liu, J. P.; Ding, R. M.; Zhu, J. H.; Li, Y. Y.; Hu, A. Z.; Li, X.; Huang, X. T. Large-scale uniform α-$Co(OH)_2$ long nanowire arrays grown on graphite as pseudocapacitor electrodes. *ACS Appl. Mater. Interfaces* **2011**, *3*, 99−103.

(15) Lu, X. H.; Zheng, D. Z.; Zhai, T.; Liu, Z. Q.; Huang, Y. Y.; Xie, S. L.; Tong, Y. X. Facile synthesis of large-area manganese oxide nanorod arrays as a high-performance electrochemical supercapacitor. *Energy Environ. Sci.* **2011**, *4*, 2915−2921.

(16) Zhang, J.; Chu, W.; Jiang, J.; Zhao, X. S. Synthesis, characterization and capacitive performance of hydrous manganese dioxide nanostructures. *Nanotechnology* **2011**, *22*, 125703−125711.
(17) Xia, H.; Feng, J. K.; Wang, H. L.; Lai, M. O.; Lu, L. MnO_2 nanotube and nanowire arrays by electrochemical deposition for supercapacitors. *J. Power Sources* **2010**, *195*, 4410−4413.
(18) Xie, K.; Li, J.; Lai, Y.; Lu, W.; Zhang, Z.; Liu, Y.; Zhou, L.; Huang, H. Highly ordered iron oxide nanotube arrays as electrodes for electrochemical energy storage. *Electrochem. Commun.* **2011**, *13*, 657−660.
(19) Sarkar, D.; Khan, G. G.; Singh, A. K.; Mandal, K. High-performance pseudocapacitor electrodes based on α-Fe_2O_3/MnO_2 core−shell nanowire heterostructure arrays. *J. Phys. Chem. C* **2013**, *117*, 15523−15531.
(20) Do, Q. H.; Fielitz, T. R.; Zeng, C.; Vanli, O. A.; Zhang, C.; Zheng, J. P. Vanadium oxide−carbon nanotube composite electrodes for energy storage by supercritical fluid deposition: Experiment design and device performance. *Nanotechnology* **2013**, *24*, 315401−315410.
(21) Qu, Q.; Zhu, Y.; Gao, X.; Wu, Y. Core−shell structure of polypyrrole grown on V_2O_5 nanoribbon as high performance anode material for supercapacitors. *Adv. Energy Mater.* **2012**, *2*, 950−955.
(22) Kim, J. W.; Augustyn, V.; Dunn, B. The effect of crystallinity on the rapid pseudocapacitive response of Nb_2O_5. *Adv. Energy Mater.* **2012**, *2*, 141−148.
(23) Wang, X.; Li, G.; Chen, Z.; Augustyn, V.; Ma, X.; Wang, G.; Dunn, B.; Lu, Y. High-performance supercapacitors based on nanocomposites of Nb_2O_5 nanocrystals and carbon nanotubes. *Adv. Energy Mater.* **2011**, *1*, 1089−1093.
(24) Wu, H.; Xu, C.; Xu, J.; Lu, L.; Fan, Z.; Chen, X.; Song, Y.; Li, D. Enhanced supercapacitance in anodic TiO_2 nanotube films by hydrogen plasma treatment. *Nanotechnology* **2013**, *24*, 455401−455407.
(25) Lokhande, C. D.; Dubal, D. P.; Joo, O. S. Metal oxide thin film based supercapacitors. *Curr. Appl. Phys.* **2011**, *11*, 255−270.
(26) Nam, K. W.; Yoon, W. S.; Kim, K. B. X-ray absorption spectroscopy studies of nickel oxide thin film electrodes for supercapacitors. *Electrochim. Acta* **2002**, *47*, 3201−3209.
(27) Xiong, S.; Yuan, C.; Zhangb, X.; Qiana, Y. Mesoporous NiO with various hierarchical nanostructures by quasi-nanotubes/nanowires/nanorods self-assembly: controllable preparation and application in supercapacitors. *CrystEngComm.* **2011**, *13*, 626−632.
(28) Zhang, X.; Shi, W.; Zhu, J.; Zhao, W.; Ma, J.; Mhaisalkar, S.; Maria, T. L.; Yang, Y.; Zhang, H.; Hng, H. H.; Yan, Q. Synthesis of porous NiO nanocrystals with controllable surface area and their application as supercapacitor electrodes. *Nano Res.* **2010**, *3*, 643−652.
(29) Oda, H.; Yamashita, A.; Minoura, S.; Okamoto, M.; Morimoto, T. Modification of the oxygen-containing functional group on activated carbon fiber in electrodes of an electric double-layer capacitor. *J. Power Sources* **2006**, *158*, 1510−1516.
(30) Kamalakar, M.V.; Raychaudhuri, A. K. Low temperature electrical transport in ferromagnetic Ni nanowires. *Phy. Rev. B* **2009**, *79*, 205417−205424.
(31) Liang, K.; Tang, X.; Hu, W. High-performance three-dimensional nanoporous NiO film as a supercapacitor electrode. *J. Mater. Chem.* **2012**, *22*, 11062−11067.
(32) Wager, C. D.; Riggs, W. M.; Davis, L. E.; Moulder, J. F.; Muilengerg, G. E. *Handbook of X-ray photoelectron spectroscopy*; Perkin-Elmer Corporation: Eden Prairie, MN, 1979; pp 74−80.
(33) Barr, T. L. An ESCA study of the termination of the passivation of elemental metals. *J. Phys. Chem.* **1978**, *82*, 1801−1810.
(34) Ovshinsky, S. R.; Fetcenko, M. A.; Ross, J. A nickel metal hydride battery for electric vehicles. *Science* **1993**, *260*, 176−181.
(35) Wang, D. C.; Ni, W. B.; Pang, H.; Lu, Q. Y.; Huang, Z. J.; Zhao, J. W. Preparation of mesoporous NiO with a bimodal pore size distribution and application in electrochemical capacitors. *Electrochim. Acta* **2010**, *55*, 6830−6835.
(36) Masarapu, C.; Zeng, H. F.; Hung, K. H.; Wei, B. Q. Effect of temperature on the capacitance of carbon nanotube supercapacitors. *ACS Nano* **2009**, *3*, 2199−2206.
(37) Patil, U. M.; Gurav, K. V.; Fulari, V. J.; Lokhande, C. D.; Joo, O. S. Characterization of honeycomb-like "β-$Ni(OH)_2$" thin films synthesized by chemical bath deposition method and their supercapacitor application. *J. Power Sources* **2009**, *188*, 338−342.
(38) Wu, Q. D.; Gao, X. P.; Li, G. R.; Pan, G. L.; Yan, T. Y.; Zhu, H. Y. Microstructure and electrochemical properties of Al-substituted nickel hydroxides modified with CoOOH nanoparticles. *J. Phys. Chem. C* **2007**, *111*, 17082−17087.
(39) Kim, J. H.; Zhu, K.; Yan, Y. F.; Perkins, C. L.; Frank, A. J. Microstructure and pseudocapacitive properties of electrodes constructed of oriented NiO-TiO2 nanotube arrays. *Nano Lett.* **2010**, *10*, 4099−4104.
(40) Kim, J. H.; Kang, S. H.; Zhu, K.; Kim, J. Y.; Neale, N. R.; Frank, A. J. Ni−NiO core−shell inverse opal electrodes for supercapacitors. *Chem. Commun.* **2011**, *47*, 5214−5216.
(41) Yuan, C.; Li, J.; Hou, L.; Zhang, X.; Shen, L.; Lou, X. W. Ultrathin mesoporous $NiCo_2O_4$ nanosheets supported on Ni foam as advanced electrodes for supercapacitors. *Adv. Funct. Mater.* **2012**, *22*, 4592−4597.
(42) Wang, D.; Li, Y.; Wang, Q.; Wang, T. Nanostructured Fe_2O_3−graphene composite as a novel electrode material for supercapacitors. *J. Solid State Electrochem.* **2012**, *16*, 2095−2102.
(43) Yan, J.; Khoo, E.; Sumboja, A.; Lee, P. S. Facile coating of manganese oxide on tin oxide nanowires with high-performance capacitive behavior. *ACS Nano* **2010**, *4*, 4247−4255.
(44) Rakhi, R. B.; Chen, W.; Cha, D.; Alshareef, H. N. Substrate dependent self-organization of mesoporous cobalt oxide nanowires with remarkable pseudocapacitance. *Nano Lett.* **2012**, *12*, 2559−2567.
(45) Xia, X.; Tu, J.; Wang, X.; Gu, C.; Zhao, X. Hierarchically porous NiO film grown by chemical bath deposition via a colloidal crystal template as an electrochemical pseudocapacitor material. *J. Mater. Chem.* **2011**, *21*, 671−679.
(46) Xu, J.; Gao, L.; Cao, J.; Wang, W.; Chen, Z. Electrochemical capacitance of nickel oxide nanotubes synthesized in anodic aluminum oxide templates. *J Solid State Electrochem* **2011**, *15*, 2005−2011.
(47) Yuan, C.; Zhang, X.; Su, L.; Gao, B.; Shen, L. Facile synthesis and self-assembly of hierarchical porous NiO nano/micro spherical superstructures for high performance supercapacitors. *J. Mater. Chem.* **2009**, *19*, 5772−5777.
(48) Kim, J. Y.; Lee, S. H.; Yan, Y.; Oh, J.; Zhu, K. Controlled synthesis of aligned Ni−NiO core−shell nanowire arrays on glass substrates as a new supercapacitor electrode. *RSC Adv.* **2012**, *2*, 8281−8285.
(49) Xia, X.; Tu, J.; Zhang, Y.; Wang, X.; Gu, C.; Zhao, X. B.; Fan, H. J. High-quality metal oxide core/shell nanowire arrays on conductive substrates for electrochemical energy storage. *ACS Nano* **2012**, *6*, 5531−5538.
(50) Lu, Q.; Lattanzi, M. W.; Chen, Y.; Kou, X.; Li, W.; Fan, X.; Unruh, K. M.; Chen, J. G.; Xiao, J. Q. Supercapacitor electrodes with high-energy and power densities prepared from monolithic NiO/Ni nanocomposites. *Angew. Chem., Int. Ed.* **2011**, *50*, 6847−6850.
(51) Nam, K. W.; Kim, K. B. A study of the preparation of NiO_x electrode via electrochemical route for supercapacitor applications and their charge storage mechanism. *J. Electrochem. Soc.* **2002**, *149*, A346−A354.
(52) Zhao, C.; Zheng, W.; Wang, X.; Zhang, H.; Cui, X.; Wang, H. Ultrahigh capacitive performance from both $Co(OH)_2$/graphene electrode and $K_3Fe(CN)_6$ electrolyte. *Sci. Rep.* **2013**, *3*, 2986−2991.
(53) Meher, S. K.; Justin, P.; Rao, G. R. Microwave-mediated synthesis for improved morphology and pseudocapacitance performance of nickel oxide. *ACS Appl. Mater. Interfaces* **2011**, *3*, 2063−2073.
(54) Selvan, R. K.; Augustin, C. O.; Berchmans, L. J.; Saraswathi, R. Combustion synthesis of $CuFe_2O_4$. *Mater. Res. Bull.* **2003**, *38*, 41−54.
(55) Ward, J. W. Spectroscopic study of the surface of zeolite Y. II. Infrared spectra of structural hydroxyl groups and adsorbed water on alkali, alkaline earth, and rare earth ion-exchanged zeolites. *J. Phys. Chem.* **1968**, *72*, 4211−4223.

(56) Wang, Y. G.; Wang, Z. D.; Xia, Y. Y. An asymmetric supercapacitor using RuO_2/TiO_2 nanotube composite and activated carbon electrodes. *Electrochim. Acta* **2005**, *50*, 5641−5646.
(57) Mai, L.; Li, H.; Zhao, Y.; Xu, L.; Xu, X.; Luo, Y.; Zhang, Z.; Ke, W.; Niu, C.; Zhang, Q. Fast ionic diffusion-enabled nanoflake electrode by spontaneous electrochemical pre-intercalation for high-performance supercapacitor. *Sci. Rep.* **2013**, *3*, 1718−1725.
(58) Luo, J. M.; Gao, B.; Zhang, X. G. High capacitive performance of nanostructured Mn−Ni−Co oxide composites for supercapacitor. *Mater. Res. Bull.* **2008**, *43*, 1119−1125.